JOURNAL OF THERMOPHYSICS AND HEAT TRANSFER
Vol. 12, No. 4, October–December 1998

Numerical Study of High-Intensity Free-Burning Arc

James Menart* and Lanchao Lin†
Wright State University, Dayton, Ohio 45435

The behavior of a free-burning argon arc including the cathode region is investigated from a theoretical perspective. Two-dimensional differential equations describing the conservation of mass, momentum, energy, and electrical current density are solved together with Ohm's law and Maxwell's equation for the magnetic field in a cylindrical coordinate system using an iterative finite volume method. Recent data of the radiative losses from an argon plasma in the form of net emission coefficients are used. Simulations are made at various electrical currents for different electrode gaps. Predicted isotherms of the arc are in fair agreement with existing experimental results. Particularly, reasonable profiles of current density at a plane beneath the cathode tip are predicted, even though nonequilibrium behavior in the cathode sheath is neglected. Comparisons of the present current density profile with reported results are made. In addition, the effect of the length scale required in the use of net emission coefficients to model the radiative characteristics of the arc is studied.

Nomenclature

B_θ = self-induced magnetic field, V s m^{-2}
C_p = specific heat at constant pressure, J kg^{-1} K^{-1}
d = electrode gap, m
e = elementary charge, 1.6×10^{-19} A s
h = enthalpy of gas mixture, J kg^{-1}
j = total current density, A m^{-2}
j_r = radial current density, A m^{-2}
j_z = axial current density, A m^{-2}
k = thermal conductivity, W m^{-1} K^{-1}
k_B = Boltzmann constant, 1.38×10^{-23} J K^{-1}
L = length scale, m
p = pressure, N-m^{-2}
r = radial coordinate, m
T = temperature, K
u = axial velocity, m s^{-1}
v = radial velocity, m s^{-1}
z = axial coordinate, m
ε_N = net emission coefficient, W m^{-3} sr^{-1}
μ = dynamic viscosity, N s m^{-2}
μ_0 = permeability of a vacuum, 1.26×10^{-6} H m^{-1}
ρ = mass density, kg m^{-3}
σ = electric conductivity, Ω^{-1} m^{-1}
ϕ = electric potential, V

Subscripts
b = boiling point
exp = experiment
m = melting point

Introduction

SEVERAL numerical simulations have been conducted for the argon high-intensity, free-burning arc. Ushio and Matsuda[1] established a two-dimensional model of the plasma arc in which the current density field is derived from existing experimental data and the radiative energy transfer is negligible. The solution of the mathematical model depends on experimental data. The two-dimensional model of Hsu et al.[2] is based on a set of conservation equations for mass, momentum, energy, and current. Solutions of the conservation equations are presented for the arc region, excluding the cathode. An exponential distribution of the current density over a plane at the cathode tip is postulated as a current density boundary condition. Cao et al.[3] performed calculations similar to Hsu et al. for a higher current and longer arc. Kovitya and Lowke[4] also solved the two-dimensional conservation equations, but used a constant current density profile over a plane at the cathode tip instead of the exponential distribution used by Hsu et al.[2] and Cao et al.[3] In addition to the numerical simulations for pure argon arcs, simulations including the effect of metallic vapor in the free-burning argon arc have been reported.[5,6] Because of the presence of a metallic vapor, the electrical conductivity, thermal conductivity, and radiant emission in the lower temperature regions of the arc are increased. The models proposed in Refs. 5 and 6 use the same exponential profile of input current density at the cathode tip as proposed by Hsu et al.[2] and do not include the cathode in their calculation domain.

In contrast to the investigations mentioned in the preceding text, the model being used in this work calculates the current density profile at the cathode tip, as opposed to having this quantity be an input to the analysis. The appropriate place to enter the boundary current density is at a location removed from the tip, where the cathode cross section is constant. At this location the current density is uniform at a value of the total current divided by the cross-sectional area of the cathode. This is similar to the manner in which Lowke et al.[7] handles the cathode current density profile. However, unlike Lowke et al., the model being used here calculates the temperature profiles in the cathode as well. This eliminates the need to resort to any experimentally measured values in the cathode region. Lowke et al. obtained their cathode temperature profiles from experimental measurements.

To calculate the current density profiles at the cathode tip in a simple manner, it is assumed that the nonequilibrium cathode sheath region can be neglected. It is possible to include the sheath region details in these types of calculations as was done by Zhu et al.[8] for a free-burning arc and by Durgapal[9] for a high current arcjet. The difficulty in doing this is the great increases in computational effort required.

As stated by other investigators,[2,7] and by the results obtained from this work, the shape of the cathode tip has a great influence on the current density profile at this location. In addition, the shape of the cathode tip influences the arc column. These influences tend to become weak at locations far removed from the cathode, but for shorter arcs, like those considered

Received Feb. 13, 1998; revision received June 17, 1998; accepted for publication June 19, 1998.

*Assistant Professor, Department of Mechanical and Materials Engineering. E-mail: jmenart@c.s.wright.edu. Member AIAA.

†Research Associate, Department of Mechanical and Materials Engineering. Member AIAA.

here, the shape of the current density profile at the cathode tip is very important. For this reason it is advantageous to have a method of determining the current density profile at the cathode tip. It is also advantageous to have a simple method because there are a number of other complexities that can be added to an analysis such as this, for example, the effects of a metal vapor in the arc. One complexity that the present authors are planning to add to this analysis is a theoretically rigorous radiative transport calculation.[10] Because of the excessively long computational time involved in such radiative transport calculations, the nonequilibrium sheath cannot be studied at the same time. This work verifies that reasonable results are obtained when the cathode sheath is neglected.

Another thing different in this analysis, as compared with many that have been done before, is that no outflow boundary condition is used. The velocity at the boundaries is taken to be zero and the boundaries are taken far enough away from the arc so that they do not influence the arc flowfield. By doing this, a numerical solution that converges more quickly is obtained.

A number of results are presented in this paper. Temperature, velocity, electrical potential, and axial current density fields for the entire arc are displayed graphically. The current density profile at the cathode, as calculated from this work, is compared with that used by Hsu et al. and that calculated by Lowke et al.[7] and Zhu et al.[8] Arc lengths of 5, 10, and 20 mm are studied. For the most part, all results are for a total arc current of 200 A, except for one graph of the temperature profile for a 300-A arc. All data are for an arc burning in a pure argon environment at 1 atm. A study of the effect of the length scale upon which the net emission coefficient is based is also made. This is done by looking at the arc centerline temperatures.

Steady-State Modeling

The argon arc configuration studied in this work, as well as the calculation domain, is shown in Fig. 1. The free-burning arc is generated between a tungsten cathode with a truncated 60-deg conical tip and a planar anode. The truncated portion of the cathode has a radius of 0.1 mm. The axisymmetric coordinate system and the dimensions of the calculation domain are given in Fig. 1. The electrode gap, d, is varied to investigate its influence on the arc characteristics.

It is assumed that the arc is in local thermodynamic equilibrium at all locations, and all thermodynamic and transport properties used are based on this assumption. All property values are taken from the work of Boulos et al.,[11] except for the net emission coefficients that come from the work of Menart et al.[12] Thermodynamic properties were determined from detailed statistical thermodynamic calculations, whereas the transport properties were determined using Sonine's polynomial expansion of the first-order Chapman–Enskog approximation of the Boltzmann equation.[13,14] Property variations with temperature are accounted for, whereas variations because of pressure are not. Many investigators show that the pressure varies by less than 2%.[2,7] In addition to temperature, net emission coefficients are also a function of some appropriately chosen length scale (Fig. 2). Menart's[10] work suggests that an appropriate length scale, L, for 200-A, 10-mm-long free-burning argon arc lies in the range from 1 to 2 mm. For regions very close to the cathode, a shorter length scale should be used. In all of this work, except the net emission coefficient length scale survey, a length scale of $L = 2$ mm is used. The net emission coefficient data of Menart et al.[12] were determined from a detailed calculation including both line and continuum radiation for neutral argon and its first two ions. Radiant energy from the entire thermal spectrum is included.

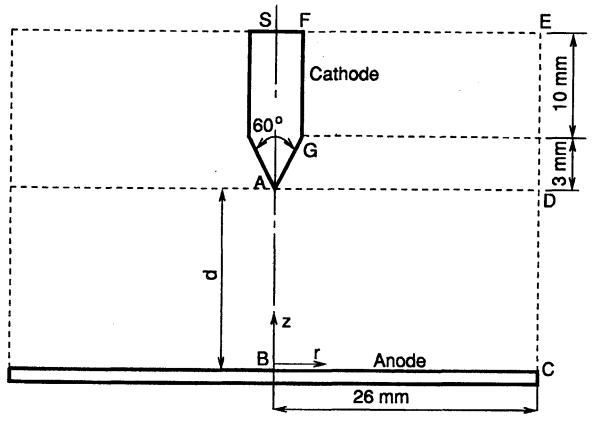

Fig. 1 Arc configuration and calculation domain.

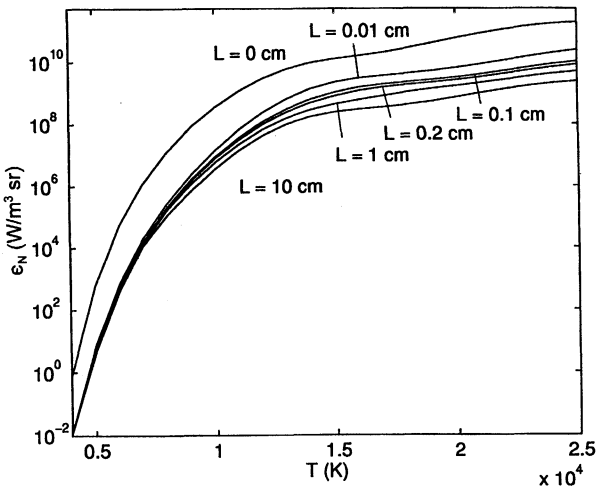

Fig. 2 Net emission coefficients for a pure argon plasma for the wavelength range of 0.03–25 μm.

Governing Equations

The two-dimensional conservation equations used to model the arc, assuming laminar flow, are expressed as follows:

Mass conservation:

$$\frac{\partial}{\partial z}(\rho u) + \frac{1}{r}\frac{\partial}{\partial r}(\rho r v) = 0 \tag{1}$$

Axial momentum conservation:

$$\rho u\frac{\partial u}{\partial z} + \rho v\frac{\partial u}{\partial r} = -\frac{\partial p}{\partial z} + 2\frac{\partial}{\partial z}\left(\mu\frac{\partial u}{\partial z}\right) + \frac{1}{r}\frac{\partial}{\partial r}\left(\mu r\frac{\partial u}{\partial r}\right) + \frac{1}{r}\frac{\partial}{\partial r}\left(\mu r\frac{\partial v}{\partial z}\right) + j_r B_\theta \tag{2}$$

Radial momentum conservation:

$$\rho u\frac{\partial v}{\partial z} + \rho v\frac{\partial v}{\partial r} = -\frac{\partial p}{\partial r} + \frac{\partial}{\partial z}\left(\mu\frac{\partial v}{\partial z}\right) + \frac{2}{r}\frac{\partial}{\partial r}\left(\mu r\frac{\partial v}{\partial r}\right) + \frac{\partial}{\partial z}\left(\mu\frac{\partial u}{\partial r}\right) - \frac{2\mu v}{r^2} - j_z B_\theta \tag{3}$$

Energy conservation:

$$\rho u\frac{\partial h}{\partial z} + \rho v\frac{\partial h}{\partial r} = \frac{\partial}{\partial z}\left(\frac{k}{C_p}\frac{\partial h}{\partial z}\right) + \frac{1}{r}\frac{\partial}{\partial r}\left(\frac{kr}{C_p}\frac{\partial h}{\partial r}\right) + \frac{j_z^2 + j_r^2}{\sigma} - 4\pi\varepsilon_N + \frac{5}{2}\frac{k_B}{e}\left(\frac{j_z}{C_p}\frac{\partial h}{\partial z} + \frac{j_r}{C_p}\frac{\partial h}{\partial r}\right) \tag{4}$$

The current density components j_z and j_r are given by Ohm's law

$$j_z = -\sigma \frac{\partial \phi}{\partial z}, \qquad j_r = -\sigma \frac{\partial \phi}{\partial r} \tag{5}$$

where the induced magnetic field effects have been neglected as well as the electron pressure gradient terms.[1–6] Neglection of these terms is often done in arcjet calculations too.[15] With these expressions and current continuity, the potential equation can be written as follows:

$$\frac{\partial}{\partial z}\left(\sigma \frac{\partial \phi}{\partial z}\right) + \frac{1}{r}\frac{\partial}{\partial r}\left(\sigma r \frac{\partial \phi}{\partial r}\right) = 0 \tag{6}$$

The self-induced magnetic field, B_θ, involved in Eqs. (2) and (3), is obtained using Maxwell's equation:

$$B_\theta = \frac{\mu_0}{r}\int_0^r j_z \xi \, d\xi \tag{7}$$

These coupled differential equations, Eqs. (1–4) and (6), are simultaneously solved to obtain the field variables u, v, p, T, and ϕ.

Boundary Conditions

As shown in Fig. 1, the closed boundaries for the calculation domain refer to SB, BC, EC, FE, and SF, and the corresponding boundary conditions are given in Table 1. At the centerline SB symmetry conditions are used. At the boundary BC the no-slip condition for the velocity is appropriate, the electrical potential is set to zero, and an enthalpy profile h_{exp} corresponding to the experimentally measured temperatures of Menart[10] is utilized. The no-slip condition for the velocity is also used at the upper boundary (SE) and the outer boundary of the cylinder (EC). This boundary condition is reasonable for a computational domain that is sufficiently large in its outer radius and height. This treatment implies that a flow of counterclockwise circulation is occurring within the calculation domain. This corresponds to physical reality in that some type of recirculation pattern needs to be established in a confined space with fluid motion. Temperatures are assumed to be 500 K at FE and EC. Conceivably, no electric current crosses the boundaries at FE and EC because of the low temperatures and, thus, low electrical conductivities. This means that $\partial\phi/\partial z = 0$ and $\partial\phi/\partial r = 0$ at these locations, respectively. At the upper boundary of the cathode (SF), the temperature is assumed to be 1000 K and a uniform current density j_0, defined by the input current divided by the cross-sectional area of the cathode, is the appropriate boundary condition for the potential equation.

Electrode-Arc Interface Treatment

Zhu et al.[8] reported that the cathode sheath is very thin and its influence on the temperature fields in the arc and on the cathode surface is small. This is important because it is the temperatures of the cathode surface and the plasma adjacent to the cathode that have a profound effect on the calculated current density distribution at the cathode tip. This is one of the reasons why the nonequilibrium cathode sheath region can be ignored in the calculation of the current density profiles and reasonable results obtained. Physically, the current density profile at the cathode is affected by the sheath region, even though it is very thin. However, the prominent feature that determines how it develops in the sheath is the temperatures on the cathode side of the sheath and the arc side of the sheath. These sheath boundary conditions have a strong influence on the shape of the current density profile that develops. This is so because the sheath is very thin and can be treated as being one dimensional.[8] Of course, to obtain highly precise distributions of the current density at the cathode, it is necessary to do a nonequilibrium analysis of the sheath. The price paid for this small increase in accuracy is greater computational time and increased complexity.

In this work, the sheath regions at both the cathode and anode are ignored. At the interface of the cathode and the arc, the harmonic mean of the transport properties is used. This treatment keeps the heat flux and current flux from the arc to the cathode relatively independent of grid size close to the interface. To avoid analyzing a sheath effect in the arc adjacent to the anode, it is assumed that the electrical conductivity maintains a constant value at this boundary, i.e., $(\partial\sigma/\partial z)_{z=0} = 0$. This is required to allow current to flow from the arc to the anode. If the electrical conductivity were allowed to follow the equilibrium values, the arc would not sustain itself. Having said this, it is believed that the actual shape of the current density profile at the anode can be determined from the shape of the current density profile just above the sheath. This is reasonable as long as the sheath region can be assumed to be one dimensional. Jenista,[16] who did a nonequilibrium analysis of the anode sheath, shows this to be the case for the current profiles within 0.5 mm of the anode.

Numerical Treatment

The governing equations (1–4) and (6), subject to the prescribed boundary conditions (see Table 1), are solved using Patankar's SIMPLER algorithm,[17] which is based on an iterative finite volume method. Arc material properties are evaluated at each grid point through the linear interpolation of tabulated material property data as a function of temperature. To avoid divergence of the calculation, the source term in the energy equation, Eq. (4), is linearized in a manner recommended by Patankar.[17]

Nonuniform grids of 58 × 82, 76 × 82, and 113 × 82 for the cases of d = 5, 10, and 20 mm, respectively, are used. Finer meshes are made in the regions close to the symmetry line, the cathode, and the anode. Because arc performance is sensitive to the cathode spot size,[7] the radius of the truncated portion of the cathode tip is determined from the experimental measurements of Zhou et al.[18] The cathode spot size derived from telemicroscopic observations indicates that the size of a cathode spot on a tungsten cathode can be approximated as a flat disk with a radius ranging from 0.1 to 0.14 mm. In this analysis, the grid size at the cathode tip is set to be 0.08 × 0.1 mm ($\Delta z \times \Delta r$).

An appropriate use of relaxation factors helps in obtaining convergent results and reduces the number of iterations required. The relaxation factors are set equal to 0.8 for velocities, 0.9–0.95 for enthalpy, and 1.0 for potentials.

Results and Discussion

Results for the calculation domain shown in Fig. 1 are presented and discussed in this section. A detailed look at the

Table 1 Boundary conditions

	SB	BC	EC	FE	SF
u	$\partial u/\partial r = 0$	$u = 0$	$u = 0$	$u = 0$	$u = 0$
v	$v = 0$	$v = 0$	$v = 0$	$v = 0$	$v = 0$
h	$\partial h/\partial r = 0$	$h = h_{exp}$	$h = h_1$ (500 K)	$h = h_1$ (500 K)	$h = h_0$ (1000 K)
ϕ	$\partial\phi/\partial r = 0$	$\phi = 0$	$\partial\phi/\partial r = 0$	$\partial\phi/\partial z = 0$	$\partial\phi/\partial z = -j_0/\sigma$

current density profiles at the cathode tip is done first. After studying the current profiles at the cathode tip, the axial current density field, the potential field, and the velocity field are presented for a 200-A, 10-mm-long arc. Temperature profiles for this arc are compared with experimental data of Hsu et al.[2] In addition to the temperature profiles for a 200-A, 10-mm-long arc, temperature plots are also shown for a 300-A, 10-mm-long arc; a 200-A, 20-mm-long arc; and a 200-A, 5-mm-long arc. These figures display the effects of increasing the total current and changing the arc length. A study of the effect on the calculations of the length scale used for the net emission coefficients is presented as well. All results presented here are for a pure argon arc burning in a 1-atm environment.

Current Density Profiles at the Cathode Tip

Figure 3 shows comparisons of the cathode tip current density profiles, $j = (j_z^2 + j_r^2)^{0.5}$, used by a number of investigators. The results from the model being presented here and those of Lowke et al.[7] are for a 5-mm-long arc, where the cathode is a truncated cone with a flat tip that has a radius of 0.1 mm. The results of Lowke et al.[7] and, from this work, using three grid points beneath the cathode tip show an off-axis peak in the current density. This occurs because of the sharp corner present at the intersection of the flat and slanted surfaces. The oscillatory behavior seen in Lowke et al.'s results is believed to be a result of numerical instabilities. The profile that Hsu et al.[2] used as their current density boundary condition is also shown. In their profile, the maximum current density at the axis is determined by assuming that all input current passes through a semispherical surface with a radius of 0.51 mm. Obviously, the present peak current density is much larger than that given by Hsu et al.

Because sharp corners in the region of the cathode spot quickly disappear when an arc is started, the off-axis peak shown in Fig. 3 will not be seen in a real arc. Sharp corners are quickly rounded off by the intense heat. To obtain the off-axis peak, the computational domain below the flat of the cathode was subdivided into three computational control volumes. When only one computational control volume is used, results as shown by the one control volume solid line in Fig. 3 are obtained. The predicted peak current density from the present model using three control volumes at the cathode tip is 2.43 $\times$ 10^4 A/cm^2, whereas that using only one control volume is 2.29 $\times$ 10^4 A/cm.[2] Therefore, using one control volume or three doesn't change the magnitude of the peak current density significantly, but it does change its position. Another set of results shown in Fig. 3 are those of Zhu et al.[8] Zhu et al. utilize a calculation routine that includes the nonequilibrium behavior of the sheath region. They consider a cathode tip similar to the one being studied here, and have results similar to those produced with this work when only one computational control volume is used beneath the flat of the cathode tip. This indicates that the present model is producing results similar to those produced with models that include a detailed account of the sheath region.

Predicted axial and radial current density profiles for the 200-A, 10-mm-long arc and the 200-A, 5-mm-long arc are shown in Fig. 4. There is very little difference between these profiles, emphasizing that the current density profile at the cathode tip is not a strong function of arc length. These curves also emphasize that the radial component of the current density is small compared with the axial component. At the symmetry axis, j_r equals zero. The radial current density, j_r, increases with r up to its maximum value at a position of approximately r = 0.17 mm, and then decreases. The axial current density continually decreases. Both j_z and j_r are essentially zero for $r >$ 2.5 mm. In association with the profiles of current densities, predicted temperatures are 3600 K at the cathode tip and 1940 K at point G on the cathode (see Fig. 1).

To see how sensitive the arc characteristics are to the radius of the flat tip, a simulation using a flat tip with a radius of 0.12 mm was carried out for a 200-A, 10-mm-long arc. The result is that the maximum axial velocity decreases by 11.6 m/s and the maximum temperature decreases by 207 K compared with the case using the flat tip of 0.1 mm radius.

Fields of Basic Parameters

Figure 5 presents contours of the axial current density for I = 200 A and d = 10 mm. Dramatic changes of the axial current density, j_z, along the z and r directions occur close to the cathode tip. Note that no current is leaving the cathode at a position significantly removed from the tip. Peak current densities that occur right at the cathode tip are not shown in Fig. 5. These can be obtained from Fig. 4. The constriction in the current density contours around the z = 2 mm location is because of a reduction of the hot core of the arc. Right next to the anode the axial current density contours become perpendicular to the anode surface. Physically, this behavior is reasonable because of the way the electrons remain at a much higher temperature than the heavy particles in the anode sheath region. Computationally, this results from the way the electric conductivity is determined at this location.

Figure 6 shows contours of electric potential for the I = 200 A arc with d = 10 mm. The contour interval is 0.5 V. The potential difference between the cathode tip and anode is 16 V, which is slightly higher than the 13.3-V computational value of Hsu et al.[2] The potential drop from the anode to the cathode cylinder is predicted to be 17 V. The total measured arc voltage

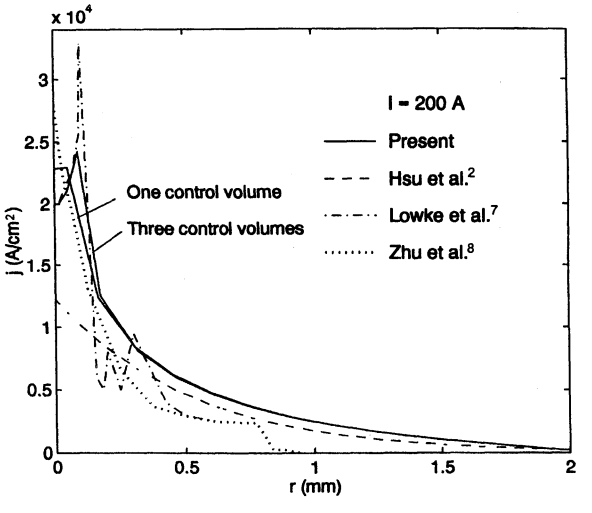

Fig. 3 Comparison of the predicted profile of current density along the line AD with reported results.

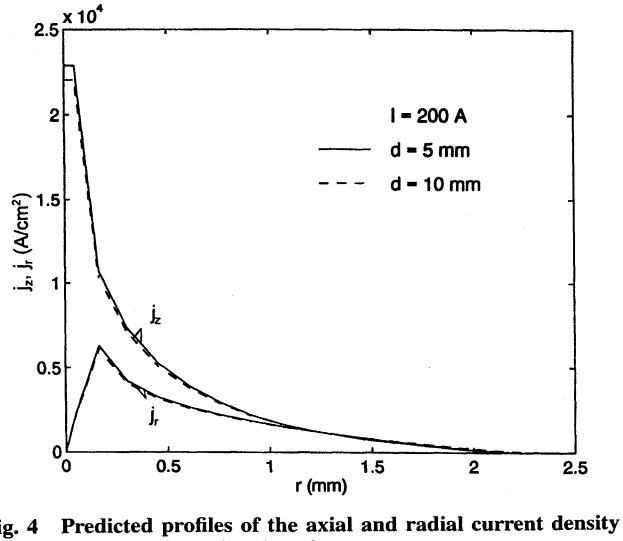

Fig. 4 Predicted profiles of the axial and radial current density along the line AD for a free-burning argon arc.

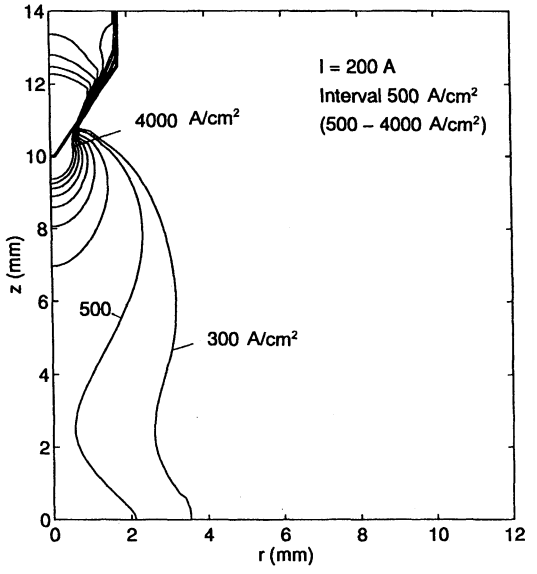

Fig. 5 Contours of axial current density for a 200-A, 10-mm-long arc.

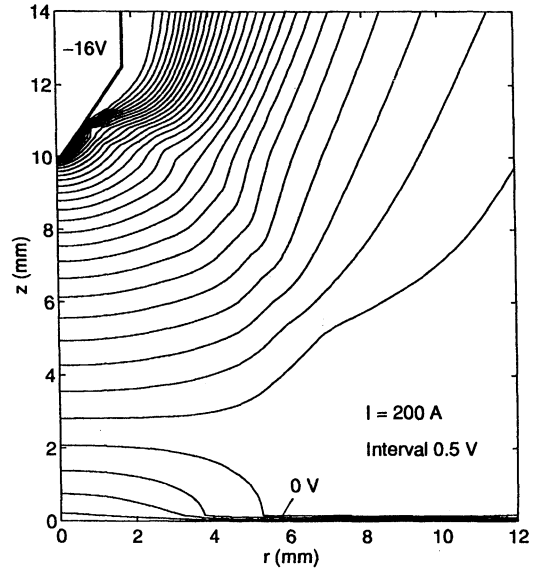

Fig. 6 Contours of electric potential for a 200-A, 10-mm-long arc.

reported by Etemadi and Pfender[19] is 16.9 V. This is in agreement with a measured value of 17 V taken by Menart.[10] This means that the calculated voltage drop in this work and experimental measurements are in good agreement. It may be thought that the calculated value should be significantly lower than the experimental value because the nonequilibrium in the sheath regions is not accounted for in this work. This is incorrect thinking for this type of model. By looking at Fig. 6, it can be seen that a significant potential drop close to the anode and cathode is predicted, particularly at the cathode. At the anode the potential gradient becomes much steeper at larger radial locations where the thermal boundary layer thickens. This is to be expected. Of course, neglecting the nonequilibrium phenomena that is occurring at the sheaths causes a slight discrepancy in the measured and calculated voltage drops.

The velocity field for I = 200 A and d = 10 mm is plotted in Fig. 7. The maximum velocity of 348.3 m/s is predicted at a location 1.84 mm down from the cathode tip. This maximum velocity is slightly larger than that predicted by Hsu et al.[2] The reason for this difference is found in Fig. 3. Hsu et al. have a

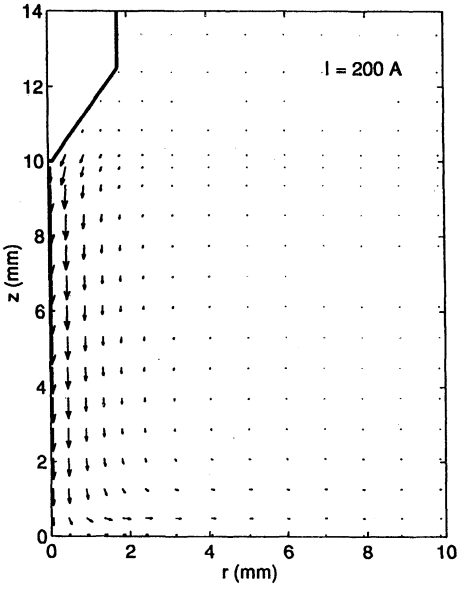

Fig. 7 Velocity field for a 200-A, 10-mm-long arc.

peak current density of 1.2×10^4 A/cm^2 compared with that of 2.29×10^4 A/cm^2 calculated in this work. Figure 7 also displays the impingement flow caused by the magnetohydrodynamic pumping effect. Flow is sucked into the arc by the magnetic fields produced by the electric current. As the flow approaches the anode, it is forced to travel in the r direction as opposed to the z direction. Close to the cylindrical outer boundary EC, the flow turns up heading back toward the boundary EF. Note that this upward flow occurs at larger radial locations than shown in Fig. 7. Near the upper boundary, the flow turns around and accelerates toward the centerline axis, forming a circular pattern. Quite obviously, recirculation occurs in every free-burning arc; it is mostly a question as to how far out radially the flow starts traveling from the anode up toward the cathode. This will be affected by the positioning of some outer wall, such as a pressure vessel. In this work we have moved the outer boundary to a large enough radial location such that the behavior in the arc located at radial locations less than 10 mm is not affected by this boundary. The outer boundary for the data in Fig. 7 is at 26 mm.

Figures 8–11 show temperature field plots for several different arcs, illustrating the effect of total arc current and arc length. Figure 8 shows a comparison between the data calculated in this work and the experimental data of Hsu et al.[2] Good comparisons are seen, except near the hottest portions of the arc. The peak temperatures determined experimentally are 21,000 K, whereas the peak temperature calculated in this work is 20,030 K at a location 0.65 mm below the cathode tip on the arc axis.

Figure 9 shows the temperature contours, with temperature intervals of 1000 K, for I = 300 A and d = 10 mm. The peak temperature in this case is 24,256 K at the same position as the calculated peak temperature shown in Fig. 8. As compared with the 200-A arc in Fig. 8, the size of the hot portion of the arc has increased. The radius of the bell-shaped formed by the 8000 K contour is 8 mm for the I = 200 A arc and 9.4 mm for the I = 300 A arc.

Figure 10 shows temperature contours for an increased electrode gap of 20 mm at I = 200 A, whereas Fig. 11 shows the same data for the decreased electrode gap of 5 mm at I = 200 A. The maximum temperature for the 20-mm-long arc is 19,490 K, which is found at a location 0.66 mm down from the cathode tip, and that for the 5-mm-long arc is 20,424 K, occurring at a location 0.65 mm down from the cathode tip. The radius of the bell-shape formed by the 8000 K contour is 10.2 mm for d = 20 mm and 6.27 mm for d = 5 mm. The

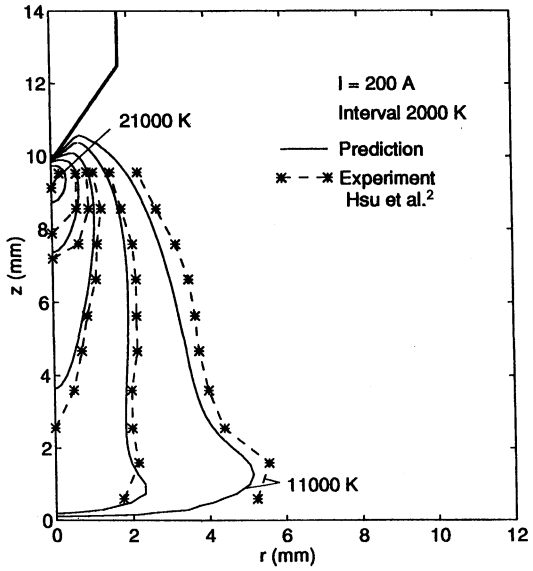

Fig. 8 Comparison of the calculated isotherms for a 200-A, 10-mm-long arc with the experimental data of Hsu et al.[2]

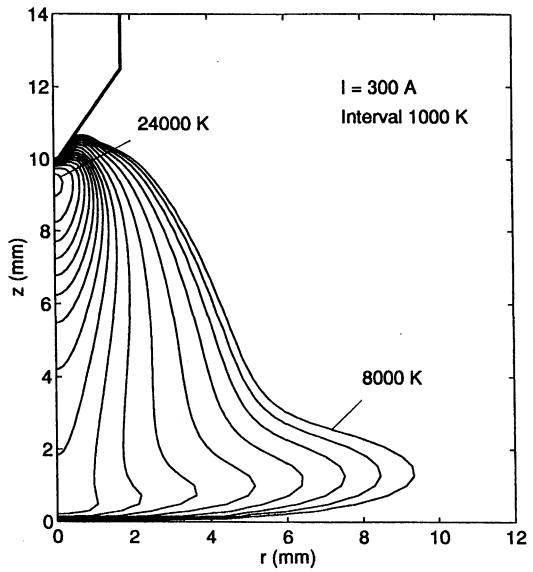

Fig. 9 Temperature contours for a 300-A, 10-mm-long arc.

corresponding value for the 10-mm arc shown in Fig. 8 is in between those of the 20 and 5 mm arcs. At a given current setting, as the arc length increases from 5 to 20 mm, the peak temperature drops slightly and the width of the bell-shaped region increases.

Effect of Length Scale

As mentioned earlier, net emission coefficients based on the length scale of $L = 2$ mm are used for the results presented in this work. To demonstrate the influence of this length scale on the arc performance, simulations are also made for $L = 0$ (optically thin condition), $L = 0.1$, and $L = 1$ mm. Variations of the temperature on the axis for three different length scales under the condition of $I = 200$ A and $d = 10$ mm are illustrated in Fig. 12. It is seen that the difference in the temperature distribution between the case of $L = 1$ mm and the case of $L = 2$ mm is small. However, the temperature for $L = 0$ is noticeably lower than the other results. The reason for this is the large difference that is seen between the $L = 0$ net emission coefficient data and that with some finite length scale. Even a very small length scale such as 0.1 mm causes a substantial drop in the net emission coefficient. This is because of the

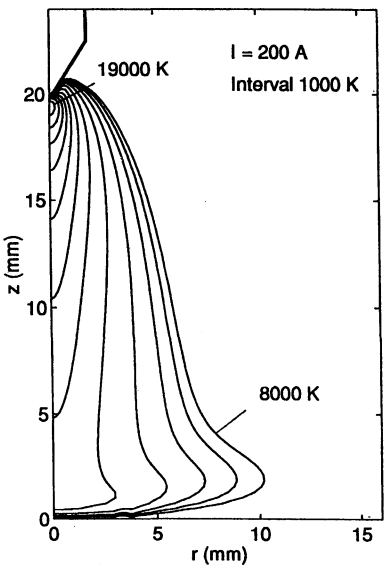

Fig. 10 Temperature contours for a 200-A, 20-mm-long arc.

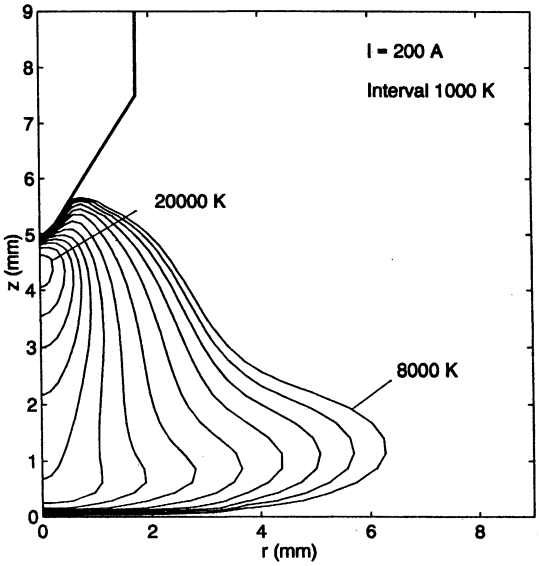

Fig. 11 Temperature contours for a 200-A, 5-mm-long arc.

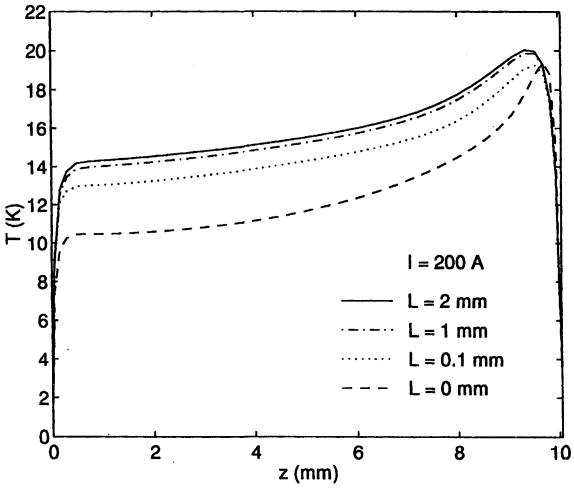

Fig. 12 Variation of temperatures on the axis of a 200-A, 10-mm-long arc for four different net emission coefficient length scales.

very short mean free path associated with radiant energy that comes from the resonance lines. From the data in Fig. 12 it can be concluded that any length scale from 1 to 2 mm could be used in this calculation. However, optically thin, $L = 0$, net emission coefficient data should not be used.

Numerical Accuracy

To estimate the influence of the cylindrical outer radius on the arc characteristics, a calculation is made for a domain having a height of 23 mm (EC) and an extended outer radius of 30 mm (SE). For the arc where $I = 200$ A and $d = 10$ mm, relative differences of the maximum axial velocity and the maximum temperature at the axis and the bell-shaped radius formed by the 8000 K temperature contour are, respectively, less than 0.5%, 0.3%, and 0.2%, compared with the case where the outer boundary is 26 mm away from the centerline. This result indicates that the behavior of the bulk of the arc is insensitive to the chosen location of the outer boundary.

A grid refinement is made for a 200-A arc with a electrode gap of 10 mm. The grid points of 76×82 used in the simulation are increased to 113×102 points, whereas the grid size at the cathode tip premains unchanged. Calculated results for the refined grid arrangement show that the maximum axial velocity changes by less than 2%, the maximum temperature by less than 1%, and the potential difference between electrodes by less than 2%. The changes are small, indicating adequate spatial discretization.

Conclusions

Reasonable profiles of current densities over a plane at the cathode tip are obtained when detailed calculations of the sheath region are neglected. A fair comparison of this profile to one that is calculated based on a model that includes details of the sheath region has been obtained. Even though the model presented here does not include sheath calculations, strong voltage drops in the region of the cathode and the anode are predicted. Comparisons between the measured and calculated total arc potential drop are in good agreement.

The axial current density at the cathode tip decreases quickly at radial locations removed from the centerline. The radial current density profiles quickly go from a value of zero to some maximum and then quickly fall back to zero. Both the radial and axial current density distributions are essentially zero at radial locations greater than 2.5 mm for the 200-A arc. At every location the magnitude of the radial current densities are much smaller than the axial values.

The peak temperature in the arc decreases with an increase of the electrode gap and increases with an increase of total arc current. The bell-shaped radius formed by the 8000 K temperature contour increases with an increase of the electrode gap spacing and an increase in the arc current for the range of parameters studied in this survey.

There is a noticeable difference between the axial temperature distribution when the length scale for the net emission coefficients is taken to be $L = 0$ or $L = 2$ mm. A smaller difference is obtained when this length scale is taken as 1 mm instead of 2 mm. Given the comparisons with experimentally measured temperature profiles, it would seem that a length scale of 1–2 mm is a reasonable choice for the 200-A, 10-mm-long free-burning argon arc.

Acknowledgment

This work was supported by a grant from the Wright State University Research Council.

References

[1]Ushio, M., and Matsuda, F., "Mathematical Modelling of Heat Transfer of Welding Arc (Part 1)," *Transactions of Japan Welding Research Institute*, Vol. 11, No. 1, 1982, pp. 7–15.

[2]Hsu, K. C., Etemadi, K., and Pfender, E., "Study of the Free-Burning High-Intensity Argon Arc," *Journal of Applied Physics*, Vol. 54, No. 3, 1983, pp. 1293–1301.

[3]Cao, M., Proulx, P., Boulos, M. I., and Mostaghimi, J., "Mathematical Modeling of High-Power Transferred Arcs," *Journal of Applied Physics*, Vol. 76, No. 12, 1994, pp. 7757–7767.

[4]Kovitya, P., and Lowke, J. J., "Two-Dimensional Analysis of Free Burning Arcs in Argon," *Journal of Physics D: Applied Physics*, Vol. 18, No. 1, 1985, pp. 53–70.

[5]Zhao, G. Y., Dassanayake, M., and Etemadi, K., "Numerical Simulation of a Free-Burning Argon Arc with Copper Evaporation From the Anode," *Plasma Chemistry and Plasma Processing*, Vol. 10, No. 1, 1990, pp. 87–99.

[6]Gonzalez, J. J., Gleizes, A., Proulx, P., and Boulos, M., "Mathematical Modeling of a Free-Burning Arc in the Presence of Metal Vapor," *Journal of Applied Physics*, Vol. 74, No. 5, 1992, pp. 3065–3070.

[7]Lowke, J. J., Kovitya, P., and Schmidt, H. P., "Theory of Free-Burning Arc Columns Including the Influence of the Cathode," *Journal of Physics D: Applied Physics*, Vol. 25, No. 11, 1992, pp. 1600–1606.

[8]Zhu, P., Lowke, J. J., and Morrow, R., "A Unified Theory of Free Burning Arcs, Cathode Sheaths and Cathodes," *Journal of Physics D: Applied Physics*, Vol. 25, No. 8, 1992, pp. 1221–1230.

[9]Durgapal, P., "Current Distribution in the Cathode Area of an Arcjet," *Journal of Thermophysics and Heat Transfer*, Vol. 7, No. 2, 1993, pp. 241–250.

[10]Menart, J., "Theoretical and Experimental Investigations of Radiative and Total Heat Transfer in Thermal Plasmas," Ph.D. Dissertation, Univ. of Minnesota, Minneapolis, MN, 1996.

[11]Boulos, M. I., Fauchais, P., and Pfender, E., *Thermal Plasmas: Fundamentals and Applications*, Vol. 1, Plenum, New York, 1994.

[12]Menart, J., Heberlein, J., and Pfender, E., "Theoretical Radiative Emission Results for Argon/Copper Thermal Plasmas," *Plasma Chemistry and Plasma Processing*, Vol. 16, No. 1, 1996, pp. 245–256 (Supplement).

[13]Hirschfelder, J. O., Curtis, C. F., and Bird, R. B., *Molecular Theory of Gases and Liquids*, Wiley, New York, 1964.

[14]Chapman, S., and Cowling, T. G., *Mathematical Theory of Non-Uniform Gases*, Cambridge Univ. Press, London, 1964.

[15]Megli, T. W., Krier, H., and Burton, R. L., "Plasmadynamics Model for Nonequilibrium Processes in N_2/H_2 Arcjets," *Journal of Thermophysics and Heat Transfer*, Vol. 10, No. 4, 1996, pp. 554–562.

[16]Jenista, J., "Numerical Model of the Anode Region of High-Current Electric Arcs," M.S. Thesis, Univ. of Minnesota, Minneapolis, MN, 1995.

[17]Patankar, S. V., *Numerical Heat Transfer and Fluid Flow*, McGraw–Hill, New York, 1980.

[18]Zhou, X., Berns, D., and Heberlein, J., "Investigation of Arc-Cathode Interaction," AIAA Paper 94-3129, June 1994.

[19]Etemadi, K., and Pfender, E., "Impact of Anode Evaporation on the Anode Region of a High Intensity Argon Arc," *Plasma Chemistry and Plasma Processing*, Vol. 5, No. 2, 1985, pp. 175–182.